



Teleseismic measurements of Upper Mantle Shear-Wave Anisotropy in Southern Mexico



Samuel Celis ^{a,*}, Luis Vázquez ^b, Raúl W. Valenzuela ^c, Laura Petrescu ^d, Xyoli Pérez-Campos ^{c,e}, Gerardo León Soto ^f

^a Posgrado en Ciencias de la Tierra, Universidad Nacional Autónoma de México, Mexico City, Mexico

^b University of Southern California, Los Angeles, CA, United States

^c Departamento de Sismología, Instituto de Geofísica, Universidad Nacional Autónoma de México, Mexico City, Mexico

^d National Institute for Earth Physics, Magurele, Ilfov, Romania

^e Comprehensive Nuclear-Test-Ban Treaty Organization, Vienna, Austria

^f Instituto de Investigaciones en Ciencias de la Tierra, Universidad Michoacana de San Nicolás de Hidalgo, Morelia, Michoacán, Mexico

ARTICLE INFO

Keywords:

Seismic anisotropy
Body waves
Subduction zone
Mantle flow
Shear-wave splitting

ABSTRACT

The Mexican subduction system is an ideal region to study 3-D mantle deformation patterns in response to changes in slab geometry and the presence of tears. Shear-wave splitting measurements were made using SKS, SKKS, and PKS waves in southern Mexico, where the Cocos slab subducts beneath the North American and western Caribbean plates. For most of southern Mexico, the results are consistent with predominantly trench-normal fast polarization directions that can be interpreted as a consequence of sub-slab entrained flow and 2-D corner flow in the mantle wedge in the presence of A-type olivine fabric (or similar). This pattern of trench-perpendicular fast axes extends northward to the region southeast of the Trans-Mexican Volcanic Belt. Beneath its eastern end, fast axes rotate $\sim 20^\circ$ clockwise and are likely controlled by the absolute motion of the North American plate. In southeastern Mexico, along the coast and above the mantle wedge tip, the fast axes are trench-normal and the delay times are the shortest. They were interpreted to result from a possibly serpentinized mantle wedge tip. In the same region above the mantle wedge core, the splitting parameters appear to result from different flow patterns in the mantle wedge and the sub-slab mantle.

1. Introduction

The Mexican subduction system is a natural laboratory to study complex convergent plate dynamics with changing slab geometry and the intricate 3-D mantle flow patterns forming in response to slab dip changes and slab tears. In southern Mexico, the oceanic Cocos plate subducts under the continental North American plate and drives upper mantle flow. Previous studies have shown that the dominant patterns of upper mantle flow are 2-D corner flow in the mantle wedge and sub-slab entrained flow (Bernal-López et al., 2016; León Soto et al., 2021; Valenzuela and León Soto, 2017; van Benthem et al., 2013). Shear-wave splitting can be used to infer the patterns of upper mantle flow (Long, 2013; Long and Silver, 2009; Long and Wirth, 2013; Savage, 1999; Silver and Chan, 1991; Teanby et al., 2004; Wüstefeld et al., 2008). This study aims to evaluate the possible existence of two slab tears; the first one was proposed by Dougherty and Clayton (2014) and Castellanos et al.

(2018), while the second one was proposed by Calò (2021) and Nava Lara and Manea (2022). Another question is the possible existence of a serpentinized mantle wedge, as proposed by Manea and Manea (2006). Lastly, this study aims to assess the possible contributions of the relative plate motion between the Cocos and North American plates or the absolute motion of the North American plate in controlling seismic anisotropy. Our new results have fundamental implications for the development of mantle flow in complex subduction settings and the role of plate motion-induced basal drag in seismic anisotropy.

Seismic anisotropy is a well-known phenomenon that produces directional dependence in shear-wave velocity. Once a shear wave propagates through an anisotropic medium, which is characterized by a lattice-preferred orientation (LPO) of minerals controlled by deformation processes, it splits into two orthogonally polarized phases that travel at different speeds: the fast and the slow wave. This partitioning is known as shear-wave splitting and can be measured using two param-

* Corresponding author.

E-mail address: samcelis93@gmail.com (S. Celis).

eters: the fast polarization direction, ϕ , and the delay time until the arrival of the slow wave, δt . The first parameter is defined by the azimuth of the direction in which the shear wave travels fastest, and the second parameter quantifies the anisotropy magnitude and depends on the dimension of the anisotropic medium, the degree of mineral alignment within it, and the inherent anisotropy of the constituent minerals (Savage, 1999; Silver and Chan, 1991; Teanby et al., 2004; van Benthem et al., 2013; Wüstefeld et al., 2008). Olivine is a major constituent of the Earth's upper mantle and is a strongly anisotropic mineral (Karato et al., 2008). When flow occurs in simple shear, the [100]-axis of olivine, which is its fast direction, becomes oriented parallel to the direction of mantle flow (Jung et al., 2006; Savage, 1999; Silver, 1996). Several olivine fabrics exist depending on the values of stress, temperature, and water content. Olivine fabrics A-, C-, D-, and E-type present the same relationship between the orientation of the olivine fast axis and flow geometry, i.e., the fast direction of olivine is oriented in the direction of mantle flow (Kneller et al., 2005; Zhang and Karato, 1995). B-type olivine fabric, i.e., wet olivine, orients its fast axis perpendicular to the mantle flow direction (Jung and Karato, 2001; Kneller et al., 2005; Long and Silver, 2009).

Core-transmitted phases, such as SKS, SKKS, and PKS, are helpful for characterizing the anisotropic structures along the receiver side of their ray path. The SKS (or similar) is a teleseismic phase that travels as a compressional wave through the liquid outer core and is then converted into a shear wave at the core-mantle boundary, which leads to a polarization in the direction of back-azimuth (Silver and Chan, 1991). Due to this conversion, all shear-wave energy should reside in the radial component, and no energy should be observed in the transverse direction. If seismic records show SKS energy on the transverse component, then seismic anisotropy may be present somewhere under the station. In most studies, anisotropy is interpreted to be located in the upper mantle (Savage, 1999; Silver, 1996; Silver and Chan, 1991).

In subduction zones, which is the case of southern Mexico, anisotropy is controlled by a complex four-layer structure: the sub-slab mantle, the slab itself, the mantle wedge, and the overriding plate, which makes it difficult to constrain the origin of the anisotropy using teleseismic data (Long and Silver, 2008). The anisotropy contribution of the slab (Faccenda et al., 2008) and the continental crust (Crampin and Chastin, 2003) to teleseismic delay times is small (Silver, 1996; Silver and Chan, 1991), so they are not considered relevant to the interpretations of this study. The classical flow model for subduction systems constitutes a 2-D behavior characterized by a subducting slab strongly coupled to the surrounding mantle, which drives corner flow in the mantle wedge and entrained flow in the sub-slab mantle, suggesting trench-normal fast polarization directions and A-type olivine fabric (or similar) for both regions (Long and Silver, 2008).

The most commonly observed orientation of fast axes from teleseismic core phases, however, is trench-parallel (Long and Silver, 2009; Long and Silver, 2008; Lynner and Long, 2013), which contradicts the predictions of the simplest 2-D entrained flow classical model. Sub-slab trench-parallel fast polarization directions are primarily controlled by 3-D trench-parallel return flow induced by trench migration combined with a barrier to entrained flow beneath the slab (i.e., top or base of the transition zone) (Faccenda and Capitanio, 2012; Long and Silver, 2008). Long and Silver (2008) documented a strong correlation between delay times and the magnitude of trench migration velocity, which holds regardless of whether the trench is advancing or retreating.

Previous studies have focused on studying seismic anisotropy beneath southern Mexico using teleseismic data. Bernal-López et al. (2016) analyzed teleseismic shear-wave splitting using records from the Meso-American Subduction Experiment (MASE) stations. They determined that fast axes in the fore-arc are trench-normal and parallel to the relative motion between the Cocos and North American plates, and fast axes in the back-arc are oriented N-S and are perpendicular to the strike of the Cocos slab. Based on their observations, they concluded that a 2-D corner flow regime prevails in the mantle wedge in the presence of A-

type olivine fabric. van Benthem et al. (2013) and Valenzuela and León Soto (2017) measured seismic anisotropy using teleseismic records from stations of Mexico's *Servicio Sismológico Nacional* (SSN, National Seismological Service) located in southern Mexico. They found trench-normal fast polarization directions parallel to the relative motion between the Cocos and North American plates where the Cocos slab subducts horizontally (Husker and Davis, 2009; Pérez-Campos et al., 2008), which they interpreted as a consequence of sub-slab entrained flow. They also observed a slight clockwise rotation of the fast axes to the east of the horizontal slab, where it starts to increase its dip, and they interpreted it as a response to an asthenospheric flow driven by the absolute motion of the North American plate. Lastly, León Soto et al. (2021) measured shear-wave splitting using teleseismic records from stations of the Veracruz-Oaxaca (VEOX) experiment deployed along the Isthmus of Tehuantepec. They found that fast axes orientations are predominantly trench normal, suggesting a 2-D corner flow in the mantle wedge and an entrained flow in the sub-slab region. Away from the trench, they observed a clockwise rotation of the fast axis orientations compared to measurements reported in the Mexican subduction zone, and they suggested that the change in orientation of the trench controls these orientations. The main purpose of this study is to understand the anisotropic structure of the upper mantle beneath southern Mexico in order to infer its mineralogical composition and the direction of mantle flow, which can then be used to interpret the geometry of the subducting Cocos slab.

2. Tectonic setting

Southern Mexico exhibits discontinuous volcanism represented by four major volcanic arcs. The Trans-Mexican Volcanic Belt (TMVB) is the largest by area. The other three are the Los Tuxtlas Volcanic Field (LTVF), the Modern Chiapanecan Volcanic Arc (MCVA), and the Central America Volcanic Arc (CAVA) (Fig. 1a). Unlike other volcanic arcs, the TMVB is not subparallel to the Middle American Trench (MAT) (Ferrari et al., 2012; Gill, 1981; Pardo and Suarez, 1995; Suarez and Singh, 1986). The reason is the existence of a flat slab that displaced the volcanic arc northward and away from the MAT (Ferrari et al., 2012; Husker and Davis, 2009; Pardo and Suarez, 1995; Pérez-Campos et al., 2008). The LTVF is located southeast of the TMVB (Nelson et al., 1995). The actual forearc region of the MCVA used to be part of the Ancient Chiapanecan Volcanic Arc (ACVA), also known as the Sierra Madre Miocene Arc, whose cessation occurred when the MCVA formed (Damon and Montesinos, 1978). Farther south, the usual subparallel configuration between the trench and the volcanic arc is restored and the CAVA stretches parallel to the MAT from southeastern Mexico toward Central America (Fig. 1a).

The Cocos plate subducts beneath the North American and the southwestern edge of the Caribbean plates in southern Mexico with a geometry that changes from northwest to southeast along the MAT, generally increasing its dip angle (Fig. 1a and b). The seismic tomography in Fig. 1b reveals these geometry changes beneath southeastern Mexico. To the northwest under Guerrero state, the Cocos slab subducts subhorizontally (Husker and Davis, 2009; Kim et al., 2010; Pardo and Suarez, 1995; Pérez-Campos et al., 2008) (Fig. 1a), where a thin (<10 km thick) zone separates the subducted oceanic crust from the continental Moho, potentially representing either a remnant mantle wedge or an altered oceanic crust (Pérez-Campos et al., 2008). According to Pérez-Campos et al. (2008), the flat slab reaches a distance of 250 km from the trench before plunging steeply into the mantle beneath the TMVB (Fig. 1a). In the region east of the flat slab, the dip angle increases from 10° to 25° (Dougherty and Clayton, 2014). The slab maintains a dip of 25° all the way to the Isthmus of Tehuantepec (IT) (Kim et al., 2011; Melgar and Pérez-Campos, 2011; Pardo and Suarez, 1995; Rodríguez-Pérez, 2007). East of the IT, the dip increases to 40° (Bravo et al., 2004; Rebollar et al., 1999) and finally reaches 45° at the Mexico-Guatemala border (Rodríguez-Pérez, 2007). Whether the dip increases gradually

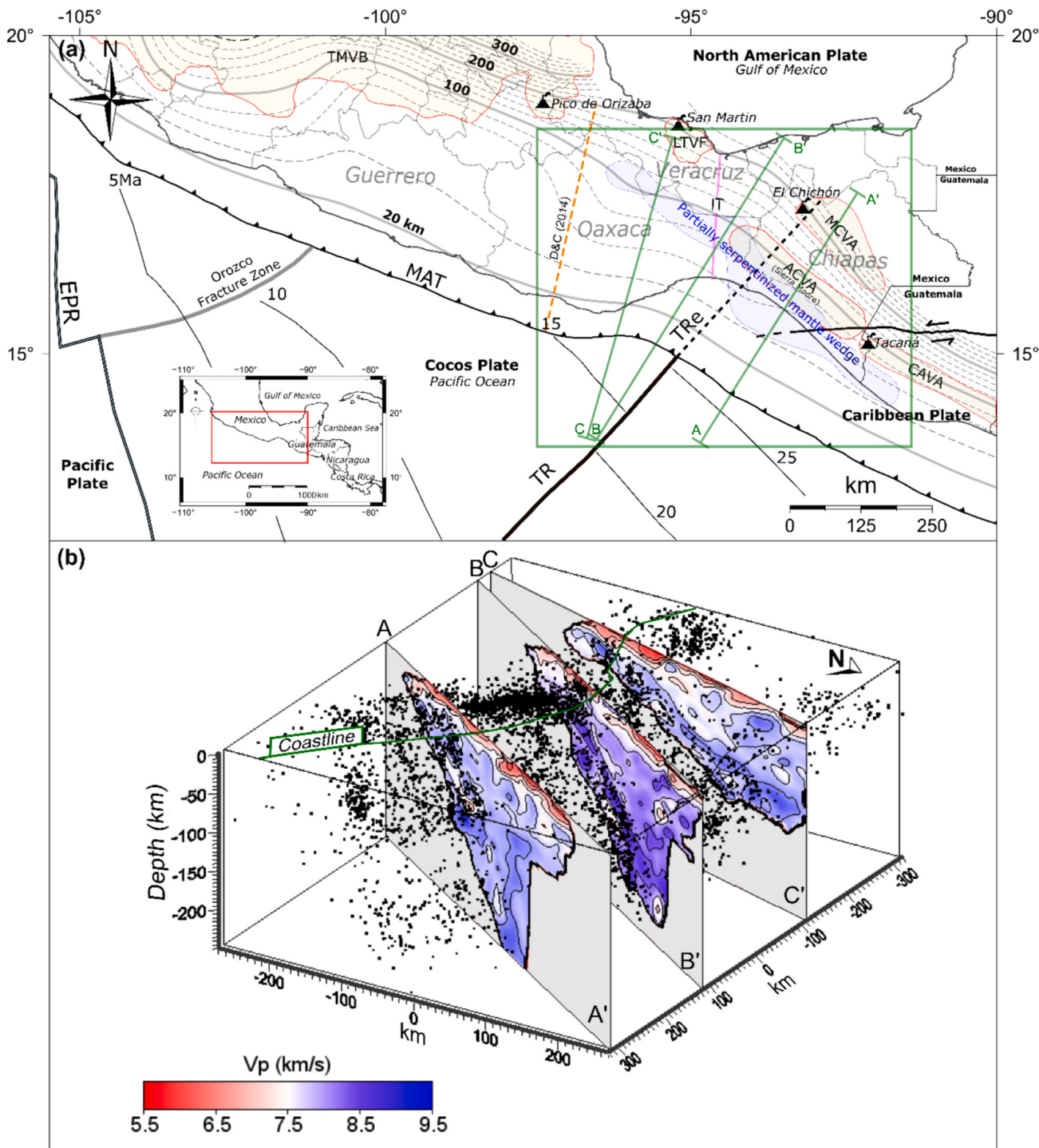


Fig. 1. Tectonic Setting. a) Tectonic features of southern Mexico. The boundaries between the Cocos, North American, Caribbean, and Pacific plates are shown. Onshore gray contours represent the Cocos slab isodepths (Hayes et al., 2018). Cocos seafloor ages are from Wilson (1996) and Manea et al. (2005a). EPR – East Pacific Rise; MAT – Middle American Trench; IT – Isthmus of Tehuantepec; TR – Tehuantepec Ridge; TRe – Tehuantepec Ridge extension. San Martin, El Chichón, and Tacaná active volcanoes are shown by smoking triangles. Red-contoured and yellow-shaded zones represent the location of volcanic belts and/or fields in the region: TMVB – Trans-Mexican Volcanic Belt, LTVF – Los Tuxtlas Volcanic Field, MCVA – Modern Chiapanecan Volcanic Arc, ACVA – the extinct Ancient Chiapanecan Volcanic Arc or Sierra Madre Miocene arc, and CAVA – Central America Volcanic Arc. The blue-shaded area represents the partially serpentinized mantle wedge proposed by Manea and Manea (2006). The orange-dashed line represents the possible slab tear proposed by Dougherty and Clayton (2014). The magenta solid line indicates the location of the Isthmus of Tehuantepec. The political limits of the states of Guerrero, Oaxaca, Veracruz, and Chiapas are shown, as well as the regional location of the study area. Green solid box encloses the region for the tomography shown in (b), while green solid lines are the profiles (A-A', B-B', and C-C') of the sections shown in (b). b) Seismic tomography model from Calò (2021) showing the variation of P-wave velocity (km/s). Black dots represent the seismic events used for the tomography, and vertical sections of P-wave velocity correspond to A-A', B-B', and C-C' profiles plotted in (a). (For interpretation of the references to colour in this figure legend, the reader is referred to the web version of this article.)

or abruptly has been a matter of debate. Several tears have been proposed for the Cocos slab for the latter scenario. In this study, we focus on two of them (Fig. 1a): one tear proposed by Dougherty and Clayton (2014) and Castellanos et al. (2018), and another one proposed by de Ignacio et al. (2003), Manea and Manea (2008), Calò (2021) and Nava Lara and Manea (2022), as we will explain below. The discontinuous nature of the four volcanic arcs may be related to the existence of the proposed tears.

A discontinuity of arc volcanism exists between the TMVB and the LTVF. Dougherty and Clayton (2014) observed an abrupt change in the dip angle from 10° to 25° while going from west to east around the eastern border of the TMVB (Fig. 1a). They attributed both the abrupt change of the dip angle and the discontinuity of arc volcanism to the existence of a possible slab tear within the downdip portion of the Cocos slab. They used a wide range of seismic methods in their comprehensive study of the slab tear. Castellanos et al. (2018) also observed this slab tear from a tomographic inversion using ambient noise. On the other hand, Fasola et al. (2016) suggest that the Cocos slab is gradually changing its dip with no evidence of a tear because they did not observe a discontinuity in the depth of the hypocenters. Additionally, they observe some continuity in the non-volcanic tremors that occur at the interface between the continental and oceanic plates. It should be noted that Fasola et al. (2016) focused their observations on the shallow end of the Cocos slab.

Another discontinuity exists between the LTVF and the MCVA. To the southeast in Oaxaca state, the Cocos slab dips at an angle of ~25° (Kim et al., 2011; Melgar and Pérez-Campos, 2011; Pardo and Suarez, 1995; Rodríguez-Pérez, 2007) near the IT (Fig. 1a). Offshore in this region, the Tehuantepec Ridge (TR) (or the Tehuantepec fracture zone) is a major bathymetric discontinuity that originates at the East Pacific Rise (EPR) and separates the Cocos plate into two segments (Manea et al., 2005b) (Fig. 1a). The TR represents a change in the age and depth of the seafloor (Fig. 1a). The age northwest of the TR is ~16 Ma (Kanjorski, 2003; Klitgord and Mammerickx, 1982) and ~ 26 Ma southeast of the TR offshore Chiapas state. The seafloor is deeper southeast of the TR (Klitgord and Mammerickx, 1982; Manea et al., 2005a, 2005b; Wilson, 1996). The Tehuantepec Ridge extension (TRe) is the TR portion subducted under the North American plate (Fig. 1a). From northwest to southeast, a change in the dip of the subducting slab from ~25° in Oaxaca to ~40° in Chiapas occurs along the TRe (Bravo et al., 2004; Rebollar et al., 1999). According to Calò (2021), the TRe induces a vertical slab tear within the subducting slab at depths exceeding 120–130 km.

Manea and Manea (2006) proposed that a continuous cooling from northwest to southeast, along with the hydration of the mantle wedge beneath the forearc region of the MCVA, produces a field of serpentine stability in the mantle wedge tip around the TRe (Fig. 1a). The continuous cooling of the mantle wedge may be due to the flat slab to the northwest, and the hydration may be caused by the dehydration of the material in the subduction channel (Hyndman and Peacock, 2003; Manea and Manea, 2006; Mookherjee and Capitani, 2011). Nava Lara and Manea (2022) concluded that the serpentinization around the TRe favors the development of a vertical slab tear coincident with this subducted bathymetric discontinuity. For slabs dipping around 45°, as in the Chiapas subduction zone, serpentine minerals (such as antigorite) produce trench-parallel anisotropy regardless of flow direction (normal or parallel) within the mantle wedge (Katayama et al., 2009). Under corner flow conditions, the serpentine is likely to be folded within the mantle wedge tip, with its [100] axis (fast axis) oriented close to vertical and its [001] axis (slow axis) oriented perpendicular to the trench, generating trench-parallel anisotropy (Mookherjee and Capitani, 2011). Under trench-parallel flow conditions, serpentine aligns its fast axis subparallel to the flow direction, thus causing an even stronger trench-parallel anisotropy (Katayama et al., 2009).

3. Data and Methods

3.1. Data

We used data from 62 permanent (SSN, 2021a; Pérez-Campos et al., 2018; Red Sísmica de Banda Ancha de Veracruz, Córdoba-Montiel et al., 2018) and temporary (the Geometry of Cocos, GECO, Rodríguez-Domínguez et al., 2019; Rapid Aftershock Deployment for the September 2017 M 8.2 and M 7.1 earthquakes in Mexico, RADSEM, Velasco and Karplus, 2017) seismic stations deployed in southern Mexico (Fig. 2). The temporary deployments operated in different periods from 2013 to 2019. We selected earthquakes with magnitudes $M_w \geq 5.9$ and epicentral distances in the 85°-140° range to ensure the SKS is isolated and not affected by the teleseismic S wave arrival energy. Data were filtered with a zero-phase Butterworth bandpass filter between 0.03 and 0.2 Hz. In some cases, the filter bandwidth was reduced in order to enhance the signal-to-noise ratio, allowing the bandpass filter to have corner frequencies of 0.04 to 0.125 Hz, which are still appropriate for the teleseismic phases (fundamental period between 10 and 20 s) used in this study and the expected delay times (Wolfe and Silver, 1998). We automatically selected and visually checked all SKS phases, and we only kept clearly visible waveforms for further analysis. The automatic selection was based on the theoretical arrival time. We also visually inspected the SKKS and PKS phases for epicentral distances >105° and included those waveforms that were clearly visible.

3.2. Covariance method

We used the Silver and Chan (1991) covariance method to measure the shear-shave splitting parameters ($\phi, \delta t$), assuming a single layer of transverse anisotropy with a horizontal axis of symmetry below the seismic station. We selected a window from the two horizontal (east-west and north-south) components with a maximum length of 42 s (depending on signal-to-noise ratio) containing the SKS at the end (Fig. 3a). Both components were rotated in the great circle arc coordinates to visually examine if energy exists on the SKS transverse component (Fig. 3b). The east-west and north-south components were rotated in 1° intervals ranging from -90° to 90°. For each one-degree step, we time-shifted one component relative to the other in 0.05 s intervals from 0 to 4 s. We calculated the covariance matrix and obtained the minimum smaller eigenvalue (λ_2^{\min}) (Silver and Chan, 1991).

Once the parameters were determined, an anisotropy correction was carried out to verify that they described the seismic anisotropy below the station. This correction consisted of two main steps: (1) in the first step, the fast and slow orthogonal phases were visually checked (Fig. 3c). (2) The second step of the correction was done by calculating the corrected radial and transverse components from the corrected fast and slow waves. For a measurement to be considered reliable, the SKS energy should be removed from the transverse component and returned to the radial component (Fig. 3b). As a consequence of the above, the original elliptical radial-transverse particle motion should be successfully linearized (Fig. 3d).

To estimate the uncertainties of the measured parameters, the 95% confidence region was determined using an inverse F test in the manner of Silver and Chan (1991) (Fig. 3e). Measurements with a well-constrained 95% confidence region were defined as good or reliable (Fig. 3), whereas poorly constrained measurements were defined as nulls. Reliable measurements for each station were averaged using the stacking method of Wolfe and Silver (1998).

4. Results

We used 62 broadband seismic stations and we were able to analyze earthquakes that occurred between 2013 and 2023. In the end, we analyzed 1427 source-to-receiver pairs and obtained 723 non-null and

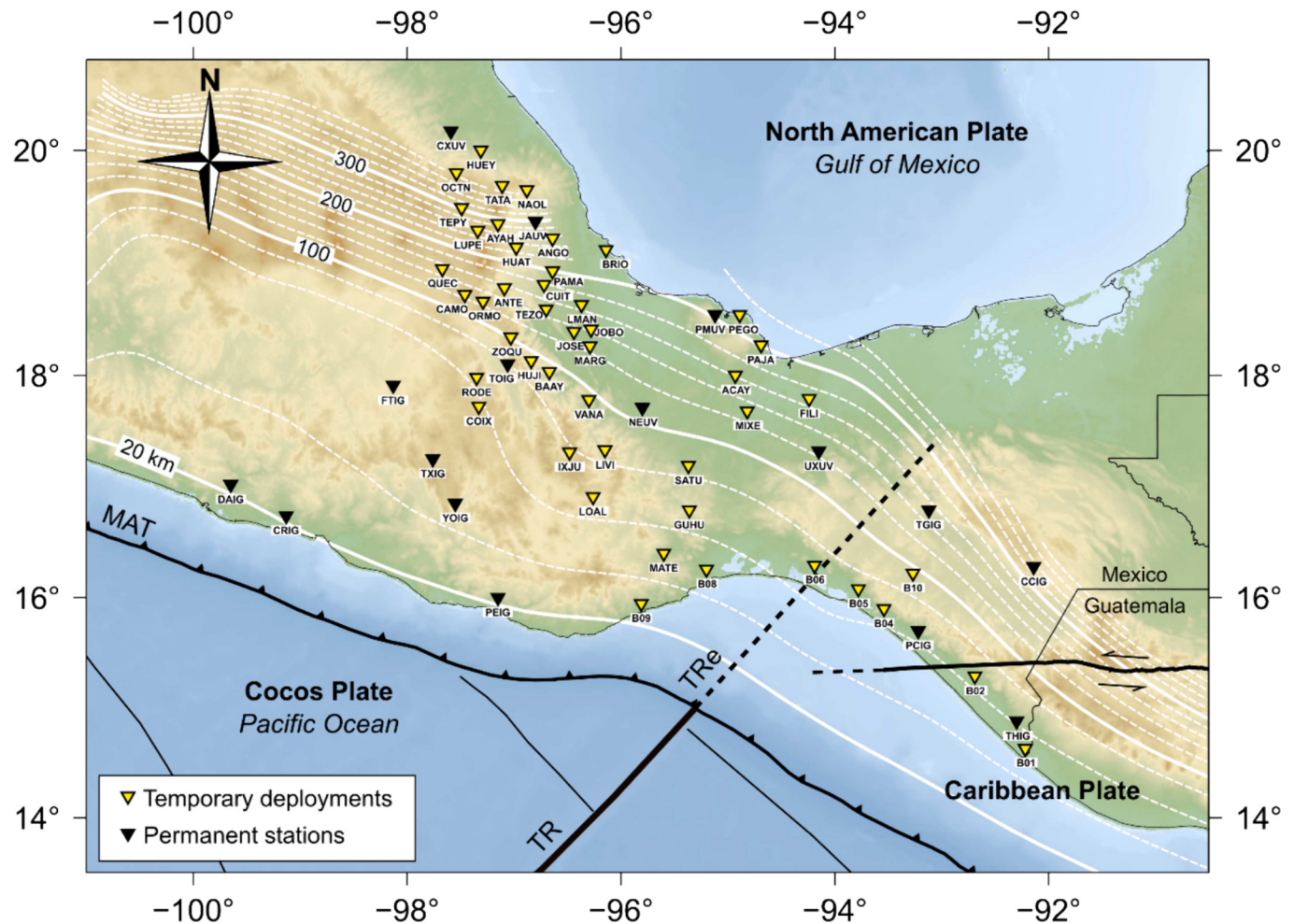


Fig. 2. Stations used to measure teleseismic shear-wave splitting to study seismic anisotropy. Stations are colour-coded according to legend. Symbols are the same as in Fig. 1.

704 null measurements. Out of the 723 measurements, 624 were made with *SKS*, 83 with *SKKS*, and 16 with *PKS* phases. The useful earthquakes recorded at each station and their resulting shear-wave splitting measurements (null and non-null) are presented in Table S1 (Supplementary Materials).

All 723 good individual measurements are shown in Fig. 4. Map from Fig. 4 reveals that almost all fast polarization directions are trench-normal (NE-SW) to the northwest while showing great variability to the southeast around the TRe. The inset in Fig. 4 shows that most measurements were made with earthquakes coming from the southwest, west, and northwest (back-azimuth $>180^\circ$). Given the geographical location of Mexico, the most useful records are from earthquakes that occurred in the southwest Pacific region.

Stacked measurements using the method of Wolfe and Silver (1998) are listed in Table S2 and shown in Fig. 5. Not all individual measurements were included in the stacking process. We calculated different stacks for each station (when it was possible), selecting for each calculation those measurements whose 95% confidence regions overlap at least in a small area. We chose the stacked results that were calculated with the greatest number of individual measurements, considering this a good way to describe the anisotropy behavior beneath each station. Some stations (e.g., TGIG, NEUV, PMUV, and UXUV) allowed us to determine two groups of shear-wave splitting parameters, appearing twice in Table S2. Those stacked measurements with large standard deviation values ($\sigma_\phi \geq 35^\circ$ and/or $\sigma_{st} \geq 0.50$ s) are reported with large uncertainty and are not interpreted in this study (red bars in Fig. 5a). Well-constrained stacked measurements are shown in Fig. 5b and are the

ones we used to make interpretations. These measurements revealed that most of the stacked fast axes are normal to the trench, which is oriented approximately N55°W. Delay times significantly decrease east of the 95°W longitude (Fig. 5b), suggesting that seismic anisotropy magnitude is smaller around the TRe than it is to the northwest of this subducted bathymetric discontinuity.

Null measurements are shown in Fig. S1. Determining the factor that could have produced the null measurements is not easy. However, in most cases, the event back-azimuth is approximately parallel or normal to the fast polarization directions measured in this study (Fig. 5), which makes it impossible to constrain the shear-wave splitting parameters and their uncertainties (Silver and Chan, 1991). The existence of multiple anisotropic layers or the absence of shear-wave splitting could also produce null measurements, which possibly correspond to those measures produced by events whose back-azimuths are neither parallel nor perpendicular to the fast axes found for each station (Barruol and Hoffmann, 1999; Silver and Chan, 1991). To study the possible existence of two or more anisotropic layers, it is necessary to have good azimuthal coverage of the events. In such cases, the shear-wave splitting parameters would be apparent and exhibit systematic variations as a function of incoming polarization with $\pi/2$ periodicity (Silver and Savage, 1994). In these cases, the calculation of stacked values can be misleading. However, it is still useful to calculate them to get a first estimation of the anisotropy. According to Rümpker and Silver (1998), in the case of two anisotropic layers, the average value of the apparent fast-axis azimuths is close to the average of the fast-axis azimuth of the two layers as long as they are not too different (maximum difference of $\sim 45^\circ$). In contrast, the

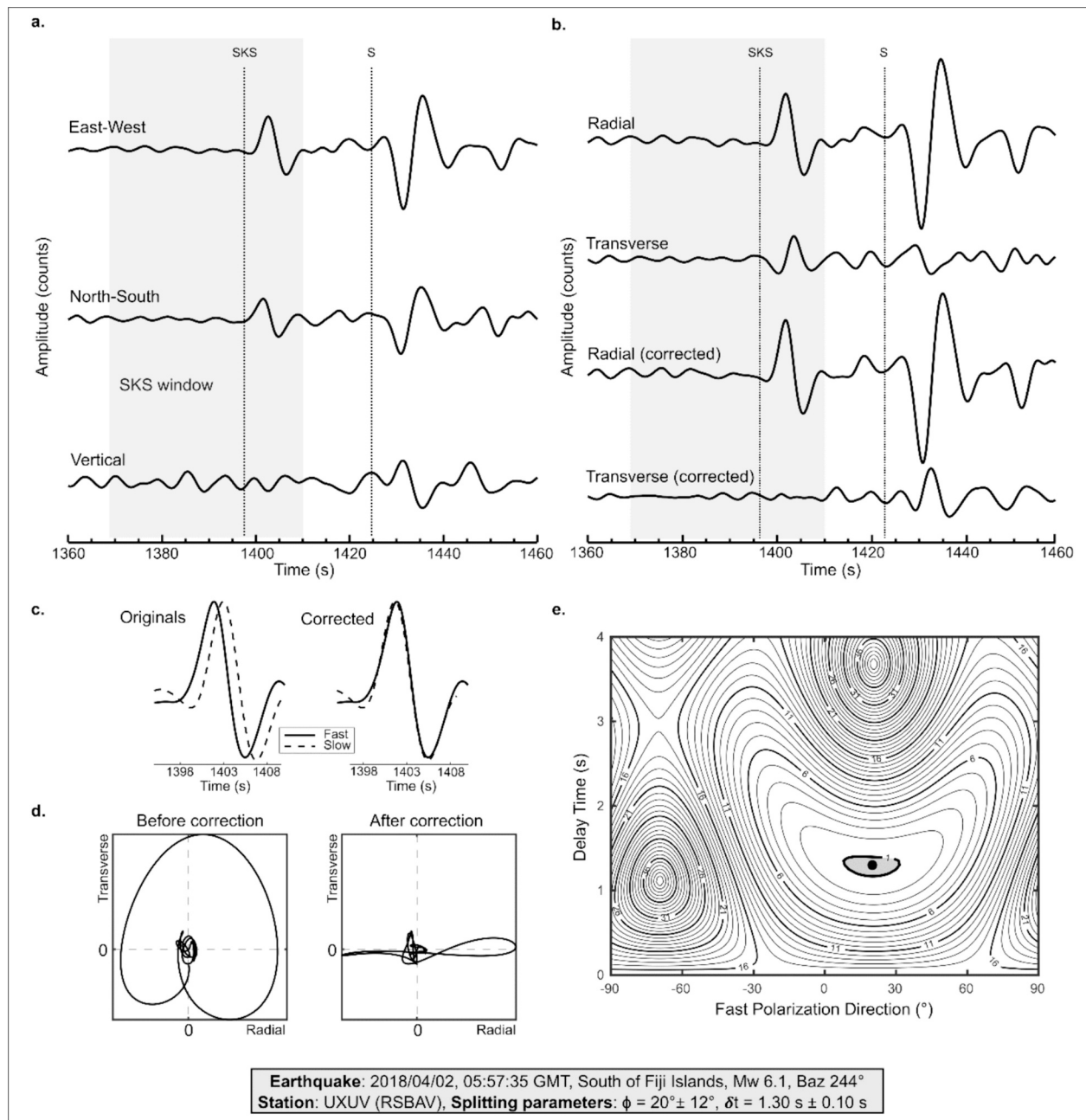


Fig. 3. Reliable shear-wave splitting measurement using the [Silver and Chan \(1991\)](#) covariance method. a. East-west, north-south, and vertical components recorded at station UXUV showing the SKS (and the S) phase from the April 2, 2018, M_w 6.1 earthquake that occurred to the south of Fiji Islands. The gray shaded area indicates the selected SKS window. b. Original (top) and corrected (bottom) radial and transverse components. It can be observed that the initial SKS transverse energy has been minimized in the corrected transverse component. c. Fast (solid line) and slow (dashed line) waves before and after the anisotropy correction. After the anisotropy correction, the fast and slow waves match. d. Particle motion before and after the anisotropy correction. The successful linearization is observed. e. Contour levels of the grid search: the gray-shaded area corresponds to the 95% confidence region, and the black dot indicates ϕ and δt values that correspond to minimum smaller eigenvalue (λ_2^{\min}).

average of the apparent delay times is equal to the sum of both splitting times.

5. Discussion

Well-constrained parameters were compared with previous teleseismic shear-wave splitting measurements reported in southern Mexico ([Fig. 6](#)). Our measurements are similar in magnitude and direction to previous results, providing a smooth spatial continuity. In general, the fast polarization directions in southern Mexico are trench-perpendicular, which is consistent with a sub-slab entrained flow and

a 2-D corner flow ([Bernal-López et al., 2016](#); [León Soto et al., 2021](#); [Valenzuela and León Soto, 2017](#); [van Benthem et al., 2013](#)). However, some patterns can be observed and will be explained below. To make the interpretations easier to understand, we classified the reliable shear-wave splitting parameters from [Fig. 5b](#) into five groups, shown in [Fig. 7](#).

5.1. Sub-slab entrained flow and corner flow

5.1.1. Subhorizontal slab (region centered at 17°N and 98°W)

Shear-wave splitting parameters measured along the MAT and in the region where the Cocos slab subducts subhorizontally ([Husker and](#)

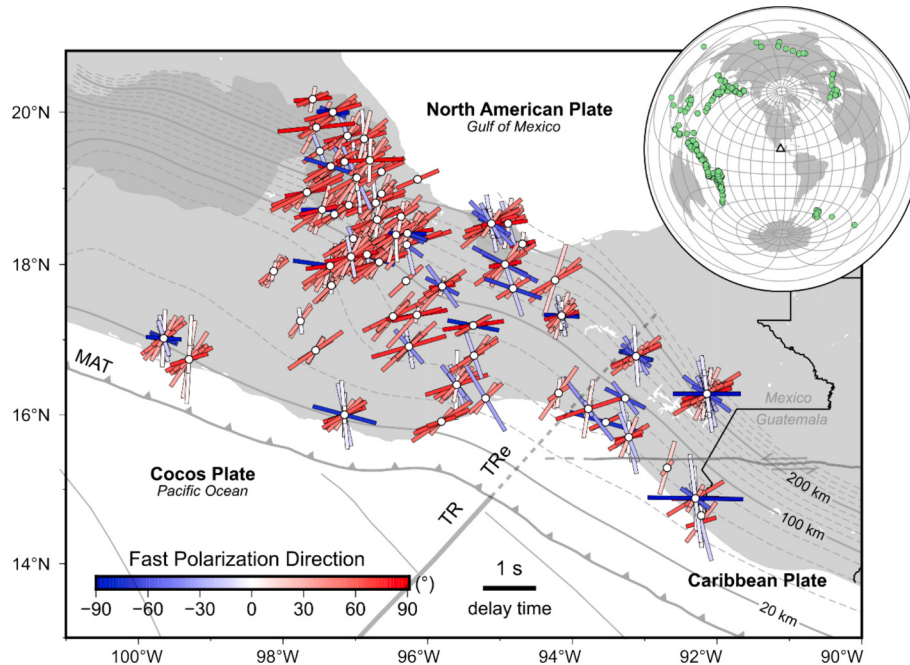


Fig. 4. Individual teleseismic splitting observations (723). The axis orientations are given by ϕ , and their lengths are proportional to δt according to legend. Fast axes are colour-coded based on the measured fast direction (from -90° to 90°). The inset top right shows the earthquakes (green circles) whose records allowed us to make reliable measurements. A station in Mexico is also included as reference (white triangle). (For interpretation of the references to colour in this figure legend, the reader is referred to the web version of this article.)

Davis, 2009; Pardo and Suarez, 1995; Pérez-Campos et al., 2008) (black bars or group 1 in Fig. 7) are approximately oriented normal to the MAT and are consistent with the ones reported by van Benthem et al. (2013) and Bernal-López et al. (2016) (Fig. 6). As shown in Fig. 7, the relative motion of the Cocos plate with respect to the North American plate has an azimuth of approximately $N30^\circ E$ (DeMets et al., 2010), and the arithmetic average of fast directions measured in this region is $\phi = 47^\circ \pm 4^\circ$; thus the fast polarization directions are approximately parallel to the Cocos plate motion relative to North America. The arithmetic average of the delay time is $\delta t = 1.32 \pm 0.20$ s, suggesting that the magnitude of the anisotropy from teleseismic phases corresponds to the upper mantle. Worldwide measurements of continental crust anisotropy have found delay times that average ~ 0.2 s (Crampin and Gao, 2006; Kaneshima, 1990; Silver, 1996; Silver and Chan, 1991). Castellanos et al. (2017) used receiver functions to measure continental crust anisotropy in the region of the flat slab in Mexico. They found delay times ranging from 0.09 to 0.24 s with an average value of 0.15 s. Likewise, for the flat slab, Castellanos et al. (2017) found delay times ranging from 0.09 to 0.27 s with an average value of 0.16 s. Besides, due to low stress, relatively high temperature, and low water content conditions in the sub-slab mantle, A-type olivine fabric is expected, which would orient its [100] axis parallel to the mantle flow direction (Jung et al., 2006; Karato et al., 2008; Kneller et al., 2005; Zhang and Karato, 1995). For these reasons, we interpret that our measurements are controlled by sub-slab entrained flow in an upper mantle made up of A-type olivine fabric. Since most of our delay times are >1 s and a thin (~ 10 km) remnant mantle wedge has been interpreted to exist between the continental crust and the flat slab (Pérez-Campos et al., 2008), we infer that the observed teleseismic anisotropy lies predominantly in the sub-slab mantle.

Two possible models can be used to explain our interpretation regarding the entrained mantle flow under the subhorizontal slab. According to the orthorhombic anisotropy model proposed by Song and Kawakatsu (2012), the sub-slab SKS fast splitting direction is controlled by both the anisotropy in the oceanic asthenosphere and the dipping angle of the slab. For shallow subduction zones (i.e., slab dip $<20^\circ$),

which is the case of this region, the fast axes tend to be oriented predominantly normal or sub-normal to the trench for vertically incident waves (such as SKS) because of the existence of horizontal melt-rich layers in the oceanic asthenosphere (Long, 2013). This mechanism can explain our trench-normal fast polarization direction observations above the subhorizontal subduction of the Cocos slab. On the other hand, Long and Silver (2008, 2009) suggest that trench-normal fast axes could be observed for young and hot subducting slabs where the thin decoupling layer between the downgoing slab and the sub-slab asthenosphere is not yet developed; thus our observations are also consistent with the absence of this decoupling layer since the Cocos slab is still young and hot (~ 15 Ma, Manea et al., 2005a) (Fig. 1).

5.1.2. Slab tear proposed by Dougherty and Clayton (2014) and Castellanos et al. (2018) (region centered at $18.5^\circ N$ and $96.5^\circ W$)

Between the TMVB and the TRe, away from the trench and above the mantle wedge core, the measured fast polarization directions are approximately normal to the trench (black bars or group 1 in Fig. 7). In this region, some stations are located above the slab tear proposed by Dougherty and Clayton (2014) and Castellanos et al. (2018), and their fast axes are on average $\phi = 37^\circ \pm 4^\circ$. This Cocos slab tear (Castellanos et al., 2018; Dougherty and Clayton, 2014) is oriented approximately SW-NE, consistent with the seismic and structural evidence presented in their studies, and is approximately parallel to our fast axis directions. In order to interpret a slab tear using the shear-wave splitting method, the existence of a vertical window along the tear through which the mantle can flow is necessary to orient the upper mantle minerals and affect the anisotropy signal. Since our anisotropy measurements are parallel to the slab tear and do not change direction to the west and east of the proposed tear, they are inconsistent with this possible tear. However, this slab tear could exist if the vertical window is not large enough for the mantle to flow through. A better spatial distribution of seismic stations could help to make a more detailed analysis of the possible slab tear.

5.1.3. Steeply-dipping slab (region centered at $17^\circ N$ and $96^\circ W$)

Southeast of the flat slab, the slab dip increases, and a mantle wedge

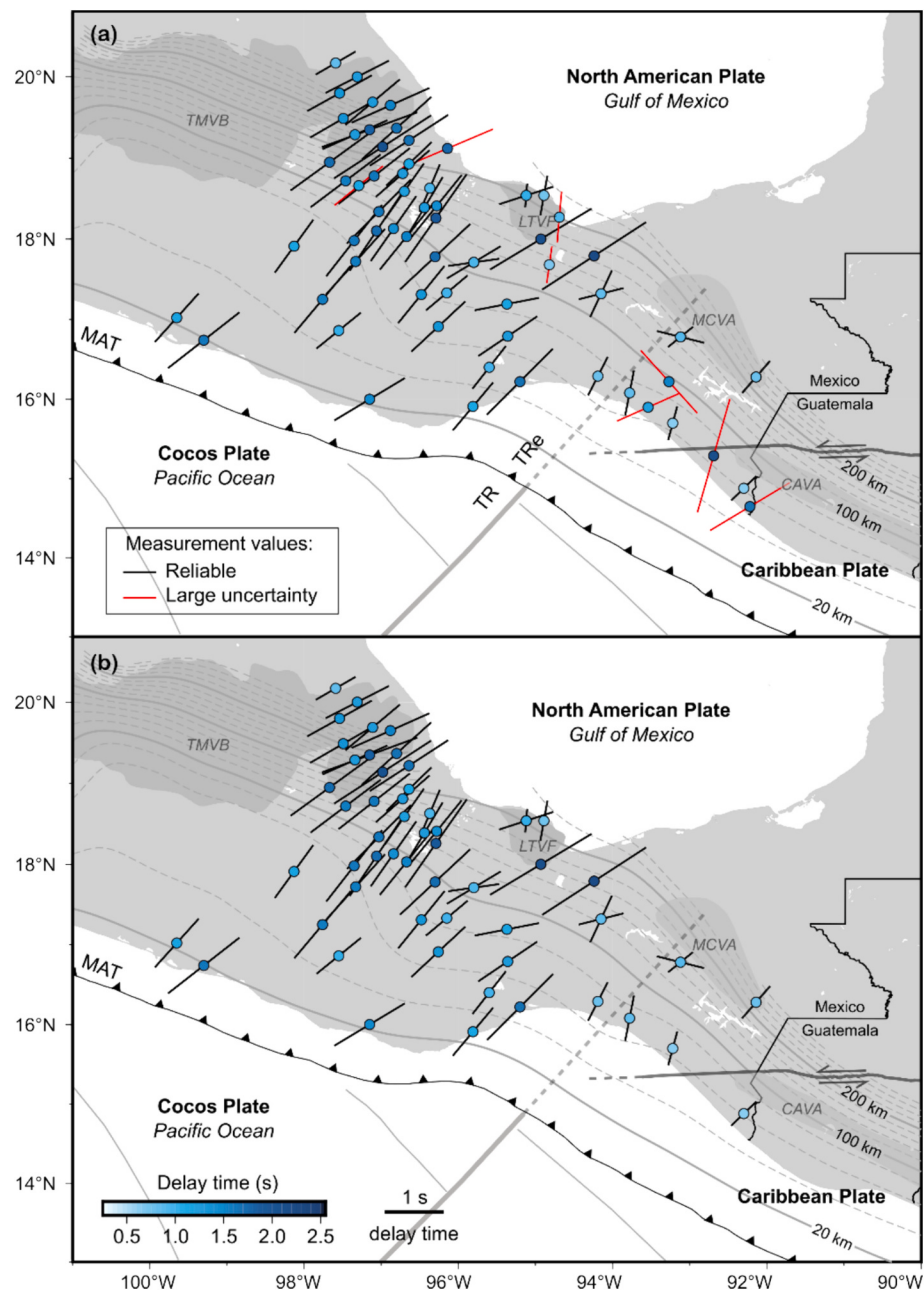


Fig. 5. Stacked shear-wave splitting parameters for each station using the method of Wolfe and Silver (1998). The length of the bars is proportional to δt , and their orientation is defined by ϕ . a) Stacked parameters, including reliable measurements (black bars) and those that present large uncertainty values (red bars). b) Only well-constrained (reliable) stacked measurements, which are the ones used for interpretations. The circles representing the stations are colour-coded according to δt in both figures. (For interpretation of the references to colour in this figure legend, the reader is referred to the web version of this article.)

develops. Shear-wave splitting parameters for this region are, on average, $(\phi, \delta t) = (47^\circ \pm 7^\circ, 1.20 \pm 0.23 \text{ s})$, and are interpreted to respond to an entrained flow in the sub-slab mantle and a 2-D corner flow in the mantle wedge, both in the presence of A-type olivine fabric. These results are consistent with Valenzuela and León Soto (2017) and van Benthem et al. (2013) (Fig. 6). The physical/chemical conditions in the mantle wedge core are more suitable for the development of A-, C-, or E-type olivine fabrics due to low stress and high temperature (Jung et al., 2006; Kneller et al., 2005). In the sub-slab mantle, we also interpreted the existence of A-type fabric due to the expected relatively high temperature, low water content, and low-stress conditions (Jung et al., 2006; Long and Silver, 2008); thus, our measured fast axes are controlled by the entrained asthenospheric flow. A couple of stations (ACAY and FILI) located northeast of this region, and near the coast of

the Gulf of Mexico, have their fast axes rotated about 10° clockwise relative to the other stations in the group and have large delay times. The clockwise rotation of the fast axes was previously observed by León Soto et al. (2021) and van Benthem et al. (2013) (Fig. 6) and is consistent with sub-slab entrained flow and 2-D corner flow in the presence of A-type olivine fabric. León Soto et al. (2021) proposed that the clockwise rotation of the MAT is responsible for the clockwise rotation of the fast axes.

5.2. Mantle flow driven by the absolute motion of North American plate

In the eastern end of the TMVB region (centered at 19.5°N and 97.5°W), measured shear-wave splitting fast axes are oblique to the strike of the slab (green bars in Figs. 7 and 8), which is approximately

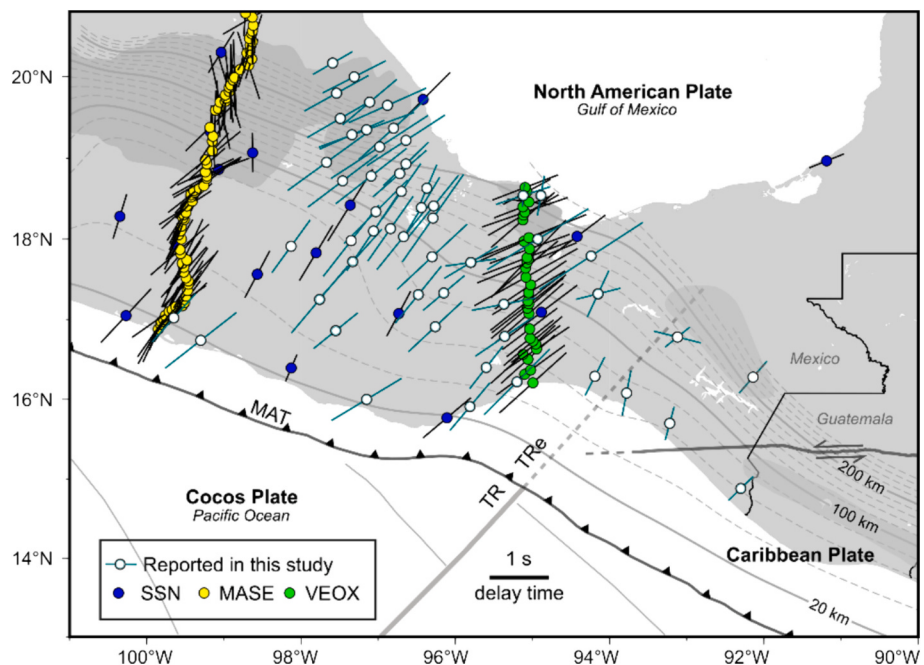


Fig. 6. Stacked shear-wave splitting parameters measured in this study compared to the ones obtained in previous SKS (or similar) splitting studies (MASE, Bernal-López et al., 2016; SSN, van Benthem et al., 2013; Valenzuela and León Soto, 2017; VEOX, León Soto et al., 2021).

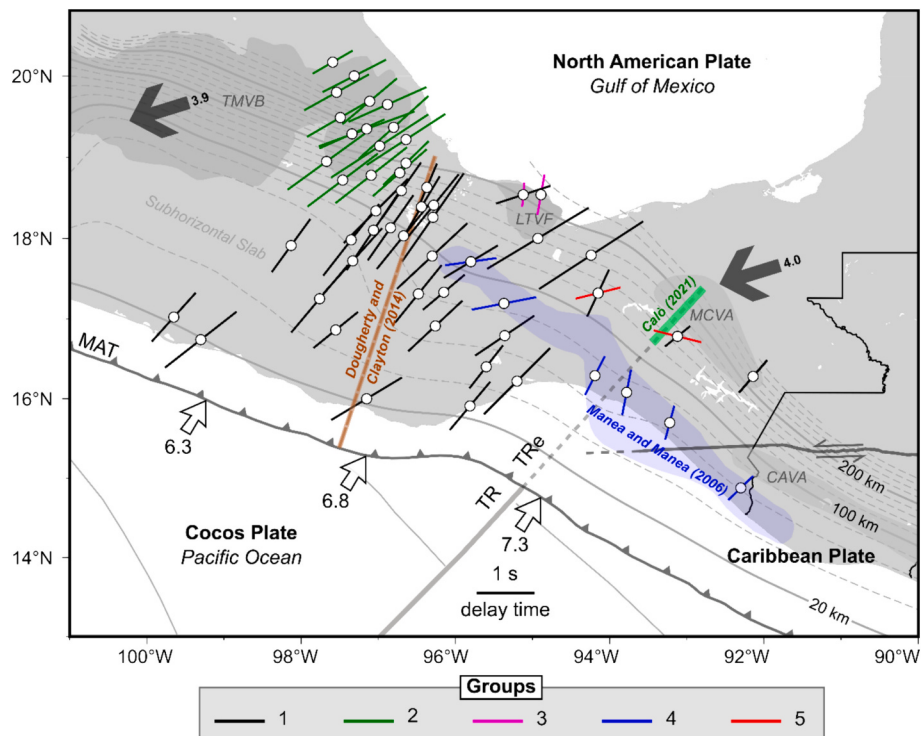


Fig. 7. Station-averaged shear-wave splitting parameters in southern Mexico classified into five different groups according to legend. The brown dashed line represents the slab tear proposed by Dougherty and Clayton (2014), the green-shaded part of the TRe corresponds to the vertical slab tear proposed by Calò (2021), and the blue-shaded area corresponds to the partially serpentinized mantle wedge proposed by Manea and Manea (2006). Dark gray arrows indicate the direction of absolute plate motion for North America (Gripp and Gordon, 2002), and white arrows indicate the direction of the plate motion of the Cocos slab relative to North America (DeMets et al., 2010); the numbers associated to the arrows correspond to velocities in cm/yr. (For interpretation of the references to colour in this figure legend, the reader is referred to the web version of this article.)

N 68° W and are on average $\phi = 57^{\circ} \pm 6^{\circ}$. This orientation suggests that the measured anisotropy does not respond to entrained mantle or 2-D corner flow. The fast axes are rotated $\sim 20^{\circ}$ clockwise with respect to

the group located south of this region (black bars in Figs. 7 and 8). This rotation may be due to a change in the direction of mantle flow as we move from south to north and away from the MAT. We propose three

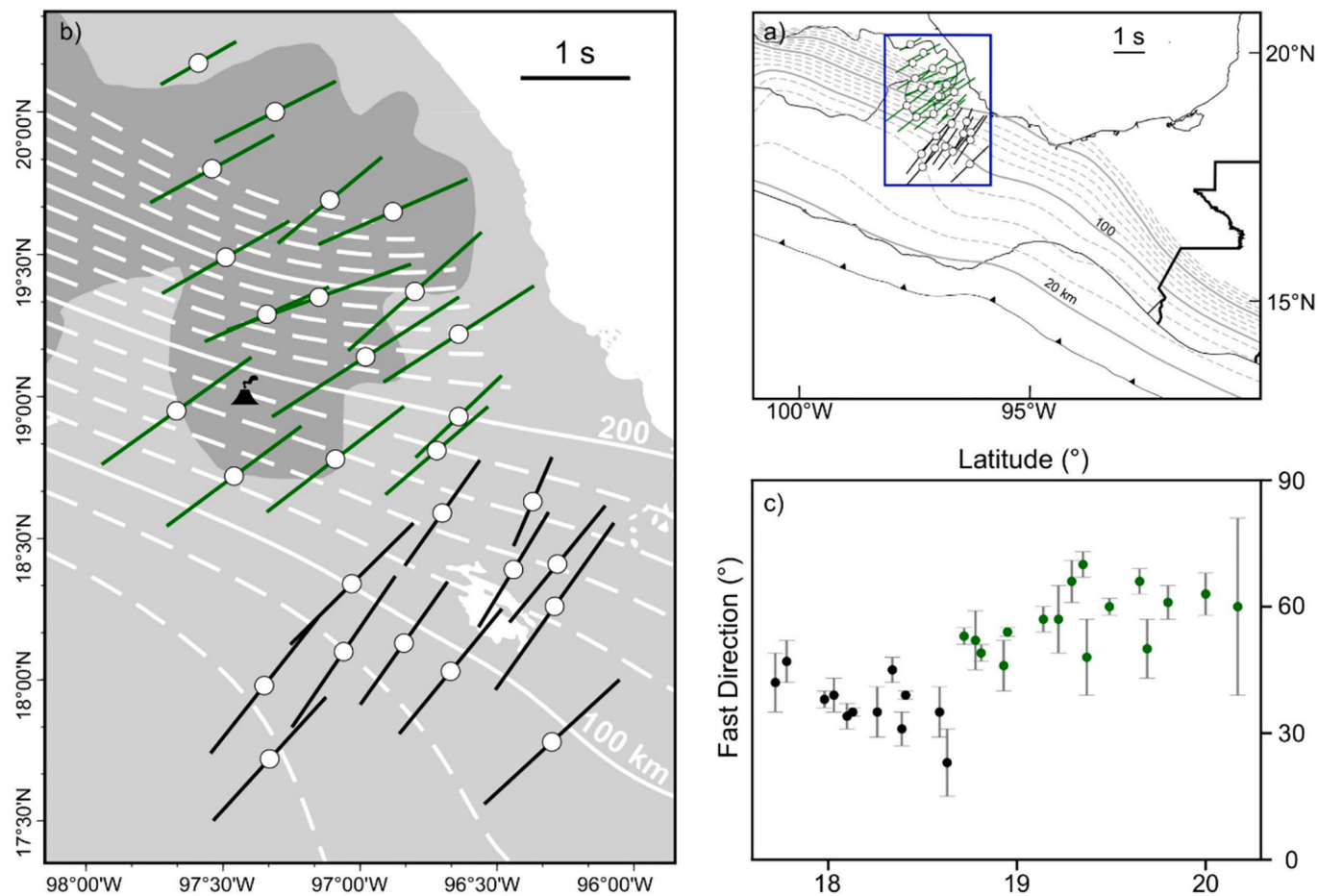


Fig. 8. Shear-wave splitting observations around the eastern end of the TMVB. a) Map showing the region where the fast axis orientations change. b) Black bars are consistent with sub-slab entrained flow and 2-D corner flow. Green bars are rotated 20° clockwise relative to black bars and are consistent with flow driven by the absolute motion of the North American plate. Black volcano symbol shows the location of the active Pico de Orizaba. c) Fast polarization directions measured for both groups plotted as a function of latitude, showing clockwise rotation of the fast axes in the northern group. The error bars represent the standard deviation for each station-stacked fast axis. (For interpretation of the references to colour in this figure legend, the reader is referred to the web version of this article.)

possible scenarios to explain the anisotropy we observed in this region. (1) Given that the fast polarization directions are approximately parallel to the absolute plate motion direction of the North American plate (Fig. 7), which is N254°E (Gripp and Gordon, 2002), we suggest that this absolute plate motion might be responsible for the observed seismic anisotropy. This scenario requires coupling between the lithosphere and the asthenosphere to allow plate-generated forces to align the olivine crystals in the asthenosphere and generate a simple, observable anisotropic signal (Silver, 1996). (2) Another possible scenario to explain our anisotropy observations in this region is the proximity to the eastern edge of the Cocos slab. One of the physical factors that could contribute to 3-D mantle flow is the proximity to slab edges, which may produce a prominent deviation from a simple 2-D corner flow pattern (Abt et al., 2009; Kincaid and Griffiths, 2004; Long and Silver, 2009; Long and Silver, 2008). The spatial coverage provided by the current stations does not show a semi-circular or toroidal pattern expected for a 3-D return flow. If more stations are deployed in the future, we may be able to test this hypothesis. Eventually, these two scenarios can act together, thus producing the strong anisotropy magnitude we observed, which is, on average, $\delta t = 1.46 \pm 0.23$ s. This high average delay time might be produced by a coherent flow in the sub-slab mantle and the mantle wedge core. For both cases, the presence of A-type olivine fabric (or similar) is required and expected due to the physical/chemical conditions of the sub-slab mantle and the mantle wedge core (Jung et al., 2006; Kneller et al., 2005; Long and Silver, 2008). (3) A third possible scenario is the existence of multiple anisotropic layers, which may

produce dependence of the shear-wave splitting parameters on the back-azimuth (Silver and Savage, 1994). However, we were not able to make a multilayer analysis in this region because we could not achieve good azimuthal coverage of the events. Based on our current data, we favor the absolute plate motion model.

5.3. Back-azimuthal variation of the splitting parameters in LTVF

In LTVF (centered at 18.5°N and 95°W, group 3 in Fig. 7), the measured shear-wave splitting parameters show a variation as a function of the back-azimuth. At station PMUV, we measured two groups of splitting parameters. (1) Using earthquakes located NW (back-azimuth $\sim 320^\circ$), we measured a fast polarization direction of $\phi = 72^\circ \pm 20^\circ$, and a delay time of $\delta t = 1.00 \pm 0.30$ s. (2) Using earthquakes located WSW (back-azimuth $\sim 250^\circ$), we measured a fast direction of $\phi = 5^\circ \pm 6^\circ$, and a delay time of $\delta t = 0.40 \pm 0.10$ s (Fig. 9). We interpret that the reason we observed these two different anisotropy patterns is a more complex structure, possibly made up of more than one single anisotropic layer or a vertical mantle flow. The first group is consistent with earlier observations using VEOX stations (León Soto et al., 2021) and with stations ACAY and FILI reported in this study (Fig. 9). In this case, we interpret that a 2-D corner flow in the mantle wedge and a sub-slab entrained flow may be controlling the orientation of the fast axes. The large delay times are consistent with this observation (León Soto et al., 2021). The fast axis of the second group is oriented approximately N-S. It is consistent with those measured at stations PEGO, MIXE, and PAJA (Fig. 9), even

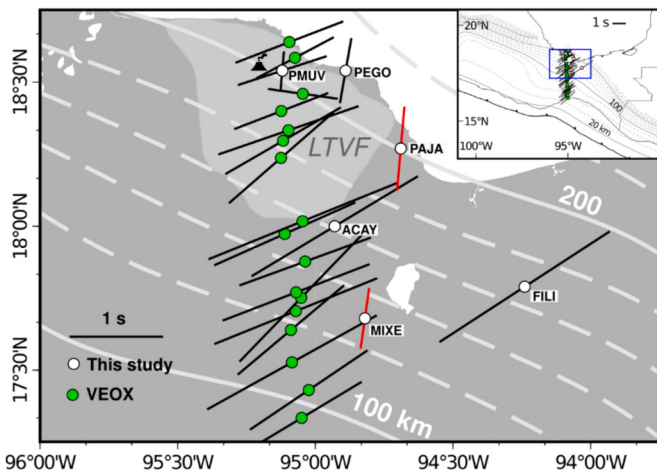


Fig. 9. Shear-wave splitting observations at LTVF. Black volcano symbol shows the location of active San Martin. Inset shows the regional location of LTVF. Two stacked shear-wave splitting parameters were found at station PMUV, as they are dependent on the back-azimuth. Red bars at MIXE and PAJA indicate large uncertainty. (For interpretation of the references to colour in this figure legend, the reader is referred to the web version of this article.)

though the latter two are reported with large uncertainties (Fig. 5a). The delay time at PMUV is small ($\delta t = 0.40 \pm 0.10$ s) and is at the limit of detection for teleseismic measurements (Silver and Chan, 1991). The shear-wave splitting technique responds to horizontal anisotropy (Silver and Chan, 1991). If the fast axes were to orient vertically, this technique would measure null or small delay times. A possible interpretation is that magma upwelling associated with volcanic activity drives vertical mantle flow. Manea et al. (2019) proposed that 8 Myr ago, an inflow of hot asthenosphere caused the Cocos slab to break, and this was responsible for starting volcanism at LTVF. It also led to lithospheric delamination of the North American plate. This event would have produced a complex mantle flow pattern under LTVF and possibly caused the observed anisotropy patterns.

5.4. Anisotropy effects of serpentinized mantle wedge

Manea and Manea (2006) proposed the existence of a partially serpentinized mantle wedge tip southeast of the flat slab. We made measurements at six stations in this area, and we believe they are consistent with the presence of serpentine minerals. Two stations are located northwest of the TRe, while the others are located southeast of the TRe (blue bars or group 4 in Fig. 7).

5.4.1. Northwest of the TRe

The stacked measurements at the two stations (NEUV and SATU) above the partially serpentinized mantle wedge are, on average, $(\phi, \delta t) = (81^\circ \pm 9^\circ, 1.03 \pm 0.15$ s), and the fast axes are oblique to the trench. If the serpentine minerals are present in the mantle wedge tip where a 2-D corner flow field dominates, then the antigorite is likely to be folded within the mantle wedge tip with its (001) plane near vertical close to the trench, thus generating trench-parallel anisotropy (Katayama et al., 2009; Mookherjee and Capitani, 2011). We believe that the anisotropic signal of the sub-slab, which has been interpreted as a result of sub-slab entrained flow, is not coherent with the signal of the mantle wedge tip in this region, which is interpreted to be produced by serpentine minerals that align their fast axes parallel to the trench. If two anisotropic layers exist below the seismic stations, then the measured splitting parameters are apparent and exhibit systematic variations as a function of incoming polarization with $\pi/2$ periodicity (Silver and Savage, 1994). However, due to the low quality of the seismic records, we could not achieve a good back-azimuthal coverage necessary for this

analysis. Based on our observations, we propose that the presence of serpentine minerals (Manea and Manea, 2006) produces an anisotropic structure in the mantle wedge that is not coherent with the sub-slab anisotropy; thus, our observations are apparent. Two groups of stacked shear-wave splitting parameters were found for one of the two stations (station NEUV) (see Table S2 and Fig. 7). The first presented a trench-normal fast axis (black colour bar) and was measured with earthquakes that occurred to the W and SW (see Table S1). The second one presented a trench-oblique fast axis (blue colour bar) and was measured with earthquakes that occurred to the NE (see Table S1). This variation with the back-azimuth may confirm the existence of the two proposed anisotropic layers (Silver and Savage, 1994).

5.4.2. Southeast of the TRe

Along the coast, above the mantle wedge tip around and southeast of the TRe, we measured shear-wave splitting parameters with four stations (B05, B06, PCIG, and THIG) that produced the shortest delay time of the study region and trench-normal fast axes (blue bars or group 4 in Fig. 7 located along the coast). These measurements are, on average, $(\phi, \delta t) = (25^\circ \pm 7^\circ, 0.69 \pm 0.14$ s). In this region, the trench is oriented $\sim 55^\circ$ W; thus, the arithmetic averaged fast axis is approximately normal to the trench. As shown in Fig. 7 and mentioned below, Manea and Manea (2006) reported the presence of a serpentinized mantle wedge ~ 125 km from and parallel to the MAT in the vicinity of the TRe. They hypothesized that the mantle wedge experiences northwest-to-southeast cooling and undergoes extensive hydration via fluids sourced from the subducted oceanic crust and subduction channel sediments, thereby reaching the serpentine stability field. The potential influence of serpentine minerals on mantle wedge anisotropy may be considerable, even when they crystallize in relatively thin layers or in a limited spatial extent (Bezacier et al., 2010; Katayama et al., 2009). In this region, the Cocos slab dips at 40° - 45° (Bravo et al., 2004; Rebollar et al., 1999; Rodríguez-Pérez, 2007) and, according to Katayama et al. (2009), the alignment of serpentine minerals within the hydrated mantle wedge results in a strong trench-parallel anisotropy for steeply ($\sim 45^\circ$) subducting slabs. This is consistent with laboratory experiments carried out by Jung (2011). If the serpentinized mantle wedge does exist, then our teleseismic shear-wave splitting parameters would be apparent and might then respond to two different anisotropic layers: a sub-slab mantle flow and a serpentinized mantle wedge. As we explained before, to make a multilayer anisotropic analysis, we need good coverage of the seismic events (Silver and Savage, 1994), which was impossible in this region due to the short recording period (~ 6 months) of the temporary stations (B05 and B06) and the low quality of the records found with the permanent stations (PCIG and THIG). However, since the seismic anisotropy differs from the observations made to the northwest, we strongly believe that an effect of a different anisotropy source exists, which could be the presence of serpentine minerals in the mantle wedge tip. Celis et al. (2024, 2022), using local intraslab earthquakes to analyze shear-wave splitting, observed trench-parallel fast polarization directions above the mantle wedge tip and interpreted that serpentine minerals are responsible for the anisotropy they observed.

5.5. Evidence of a possible slab tear along the TRe

Around the TRe and above the mantle wedge core, we found two groups of stacked shear-wave splitting parameters at each of two stations, UXUV and TGIG. This observation may signal the presence of multiple anisotropic layers (Silver and Savage, 1994). One group is oblique to the trench and is, on average, $(\phi, \delta t) = (90^\circ \pm 11^\circ, 0.83 \pm 0.10$ s) (group 5 or red bars around the TRe in Fig. 7), while the other one is normal to the trench and is, on average, $(\phi, \delta t) = (38^\circ \pm 3^\circ, 0.73 \pm 0.15$ s) (black bars for the same stations in Fig. 7). For station CCIG, the fast polarization direction is trench-perpendicular (black bar in Fig. 7). The existence of a vertical slab tear along the TRe at depths

>120–130 km has been proposed (Calò, 2021; Nava Lara and Manea, 2022). This tear could possibly cause sub-slab mantle material to flow around the steeper slab edge, through the vertical window between the slab edges, and into the mantle wedge southeast of the TRe. Given the different dip angles across the TRe (25° to the northwest, Pardo and Suarez, 1995; Rodríguez-Pérez, 2007; Kim et al., 2011; Melgar and Pérez-Campos, 2011; and ~40° to the southeast, Rebollar et al., 1999; Bravo et al., 2004) and also the different slab rollback rates, a 3-D toroidal flow around the edge of the steeper-dipping slab is expected (Long and Silver, 2008). If a 3-D toroidal flow is occurring around the TRe, then the measured splitting parameters at stations UXUV, TGIG, and CCIG are apparent and might be responding to a multilayer anisotropy configuration (Fig. 7). Furthermore, the fact that the mantle wedge is larger and the delay times are shorter southeast of the TRe may be evidence that the anisotropic structure is different from the one observed to the northwest of the TRe. Celis et al. (2024, 2022) used local intraslab earthquakes and observed a 3-D trench-parallel mantle flow in the mantle wedge southeast of the TRe. Therefore, the anisotropy patterns observed in this study from core-refracted shear-wave phases could be in agreement with this scenario. Unfortunately, due to the limited back-azimuthal coverage, it was not possible to carry out a multilayer inversion in the manner of Frederiksen and Bostock (2000) and Silver and Savage (1994) at these stations.

6. Conclusions

Teleseismic shear-wave splitting measurements using phases such as SKS, SKKS, and PKS have been presented and are consistent with previous results in the same region. The observed anisotropy is controlled by the geometry of the subducting slab and, in general, measured fast polarization directions are consistent with sub-slab entrained flow and mantle wedge 2-D corner flow in the presence of A-type (or similar) olivine fabric, with some regional patterns that can be interpreted based on changes in mantle flow direction and/or mineralogy.

In the region of the flat slab, our measurements are consistent with a sub-slab entrained flow that can be controlled by a strong coupling between the sub-slab asthenosphere mantle and the subducting Cocos slab or by the existence of horizontal melt-rich layers in the oceanic lithosphere. Due to physical/chemical conditions, such as low stress, relatively high temperatures, and low water content, which are expected in the sub-slab mantle, we infer the presence of A-type olivine fabric with its fast axis oriented parallel to the mantle flow direction.

In the region between the eastern end of the TMVB and the LTVF, the fast polarization directions are normal to the trench. We interpret that these respond to a sub-slab entrained flow and a 2-D corner flow in the mantle wedge in the presence of A-type olivine fabric (or similar). Our measurements do not suggest a change in the pattern of mantle flow at the slab tear location proposed by Dougherty and Clayton (2014) and Castellanos et al. (2018). However, an incipient tear that has not yet developed a large enough window to allow mantle to flow through it might exist.

In the region above the eastern end of the TMVB, the fast axes are rotated ~20° clockwise relative to other stations immediately to the south. We propose that seismic anisotropy parameters are controlled either by the absolute motion of the North American plate or by a toroidal flow due to the proximity to the eastern edge of the Cocos slab in the presence of A-type olivine fabric.

We measured shear-wave splitting parameters with stations located above the region of the partially serpentinized mantle wedge proposed by Manea and Manea (2006). We observed a deviation of the fast polarization directions in the northern part of the region and a significant reduction in delay times in the southern part. We attributed these changes to the presence of a second anisotropic layer, which we interpret as the serpentinized mantle wedge. For this reason, we propose that the observed splitting parameters are apparent and consistent with the possible existence of two anisotropic layers: the sub-slab mantle and the

serpentinized mantle wedge. Additionally, we found shear-wave splitting parameters in the mantle wedge core and around the TRe that are not consistent with the ones measured to the northwest. We interpret that they could also be responding to a multilayer anisotropic configuration with different mantle flow patterns in the mantle wedge and sub-slab region, possibly due to the existence of a vertical tear in the Cocos slab along the TRe (Calò, 2021; Nava Lara and Manea, 2022). Unfortunately, due to the limited back-azimuthal coverage, we were not able to make a multilayer anisotropic analysis in this region.

CRediT authorship contribution statement

Samuel Celis: Writing – review & editing, Writing – original draft, Software, Methodology, Investigation, Formal analysis, Conceptualization. **Luis Vázquez:** Writing – review & editing, Software, Methodology, Investigation. **Raúl W. Valenzuela:** Writing – review & editing, Validation, Supervision, Methodology, Investigation, Formal analysis, Conceptualization. **Laura Petrescu:** Software, Methodology, Investigation, Conceptualization. **Xyoli Pérez-Campos:** Writing – review & editing, Validation, Supervision, Resources, Project administration, Funding acquisition, Conceptualization. **Gerardo León Soto:** Methodology, Investigation, Conceptualization.

Declaration of competing interest

The authors declare the following financial interests/personal relationships which may be considered as potential competing interests:

Samuel Celis reports financial support was provided by CONACYT. If there are other authors, they declare that they have no known competing financial interests or personal relationships that could have appeared to influence the work reported in this paper.

Data availability

SSN and RSBAV data are available through SSN (2021b) (<https://doi.org/10.21766/SSNMX/SN/MX>). Data from the Rapid aftershock deployment for the September 2017 M = 8.2 and M = 7.1 earthquakes in Mexico (RADSEM; Velasco and Karplus, 2017) can be downloaded from the Incorporated Research Institutions for Seismology Consortium Data Management Center (IRIS-DMC) (<http://service.iris.edu/fdwns/dataset/1/>), the seismic network code is ZB. The GECO network data can be requested from X. Pérez-Campos (xyoli@igeofisica.unam.mx). Topography and bathymetry grids were provided by Amante and Eakins (2009).

Acknowledgements

We are grateful to Servicio Sismológico Nacional (SSN) staff for station maintenance and data acquisition and distribution. We are also thankful to Francisco Córdoba and Centro de Ciencias de la Tierra de la Universidad Veracruzana (CCTUV), as well as the Civil Defense staff of Veracruz state (SPC-VER), for the data from Red Sísmica de Banda Ancha de Veracruz (RSBAV), and Allen Husker and Aaron Velasco for the data from Rapid Aftershock Deployment for the September 2017 M = 8.2 and M = 7.1 Earthquakes in Mexico (RADSEM). The Geometry of Cocos (GECO) deployment was funded by Consejo Nacional de Humanidades, Ciencia y Tecnología (CONAHCYT) through project 177676, and Universidad Nacional Autónoma de México (UNAM) through Programa de Apoyos a Proyectos de Investigación e Innovación Tecnológica (PAPIIT) grants IN106119 and IN110822 to Xyoli Pérez-Campos, and IN102618 to Arturo Iglesias. S. C. is grateful for a CONAHCYT Ph.D. scholarship. L. P. is supported by the Nucleo project no. PN23360201. We thank Marco Calò for providing Fig. 1b, showing the seismic tomography model. Some figures were made using the Generic Mapping Tools (GMT) package (Wessel and Smith, 1998). This work was supported by UNAM-PAPIIT grant IN110822. We thank Editor Gregory

Houseman and two anonymous reviewers for their valuable suggestions, which greatly improved the manuscript. The views expressed herein are those of the authors and do not necessarily reflect the views of the CTBTO Preparatory Commission.

Appendix A. Supplementary data

Supplementary data to this article can be found online at <https://doi.org/10.1016/j.tecto.2024.230465>.

References

- Abt, D.L., Fischer, K.M., Abers, G.A., Strauch, W., Protti, J.M., González, V., 2009. Shear wave anisotropy beneath Nicaragua and Costa Rica: Implications for flow in the mantle wedge. *Geochemistry Geophys. Geosystems* 10. <https://doi.org/10.1029/2009GC002375>.
- Amante, C., Eakins, B.W., 2009. ETOPO1 1 arc-minute global relief model: procedures, data sources and analysis. In: NOAA Tech. Memo. NESDIS NGDC-24 Natl. Geophys. Data Center, NOAA. <https://doi.org/10.7289/V5C8276M> [01/08/2022].
- Barroso, G., Hoffmann, R., 1999. Upper mantle anisotropy beneath the Geoscope stations. *J. Geophys. Res. Solid Earth* 104, 10757–10773. <https://doi.org/10.1029/1999jb900033>.
- Bernal-López, L.A., Garibaldi, B.R., León Soto, G., Valenzuela, R.W., Escudero, C.R., 2016. Seismic Anisotropy and Mantle Flow Driven by the Cocos Slab under Southern Mexico. *Pure Appl. Geophys.* 173, 3373–3393. <https://doi.org/10.1007/s0024-015-1214-7>.
- Bezacier, L., Reynard, B., Bass, J.D., Sanchez-valle, C., Van De Moortèle, B., 2010. Elasticity of antigorite, seismic detection of serpentinites, and anisotropy in subduction zones. *Earth Planet Sci. Lett.* 289, 198–208. <https://doi.org/10.1016/j.epsl.2009.11.009>.
- Bravo, H., Rebollar, C.J., Uribe, A., Jimenez, O., 2004. Geometry and state of stress of the Wadati-Benioff zone in the Gulf of Tehuantepec, Mexico. *J. Geophys. Res.* 109, B04307 <https://doi.org/10.1029/2003JB002854>.
- Calò, M., 2021. Tears, windows, and signature of transform margins on slabs. Images of the Cocos plate fragmentation beneath the Tehuantepec isthmus (Mexico) using Enhanced Seismic Models. *Earth Planet. Sci. Lett.* 560. <https://doi.org/10.1016/j.epsl.2021.116788>.
- Castellanos, J., Pérez-Campos, X., Valenzuela, R., Husker, A., Ferrari, L., 2017. Crust and upper-mantle seismic anisotropy variations from the coast to inland in central and Southern Mexico. *Geophys. J. Int.* 210, 360–374. <https://doi.org/10.1093/gji/ggx174>.
- Castellanos, J.C., Clayton, R.W., Pérez-Campos, X., 2018. Imaging the Eastern Trans-Mexican Volcanic Belt with Ambient Seismic Noise: evidence for a Slab Tear. *J. Geophys. Res. Solid Earth* 123, 7741–7759. <https://doi.org/10.1029/2018JB015783>.
- Celis, S., Valenzuela, R.W., León Soto, G., Pérez-Campos, X., 2022. Upper mantle and continental crust anisotropy in southeastern Mexico determined from shear-wave splitting measurements using local intraslab earthquakes. *J. South Am. Earth Sci.* 119, 104023. <https://doi.org/10.1016/j.jsames.2022.104023>.
- Celis, S., Valenzuela, R.W., Calò, M., Pérez-Campos, X., León Soto, G., 2024. Anisotropic structure in the mantle wedge beneath southeastern Mexico from shear-wave splitting tomography. *J. Geodyn.* 159 <https://doi.org/10.1016/j.jog.2023.102007>.
- Córdoba-Montiel, F., Iglesias, A., Pérez-Campos, X., Síeron, K., Valdés-González, C., Singh, S.K., Pacheco, J.F., 2018. The Broadband Seismological Network of Veracruz, Mexico: toward a Regional Seismotectonic Interpretation. *Seismol. Res. Lett.* 89, 345–355. <https://doi.org/10.1785/0220170195>.
- Crampin, S., Chastin, S., 2003. A review of shear wave splitting in the crack-critical crust. *Geophys. J. Int.* 155, 221–240.
- Crampin, S., Gao, Y., 2006. A review of techniques for measuring shear-wave splitting above small earthquakes. *Phys. Earth Planet. Inter.* 159, 1–14. <https://doi.org/10.1016/j.pepi.2006.06.002>.
- Damon, P.E., Montesinos, E., 1978. Late Cenozoic volcanism and metallogenesis over an active Benioff zone in Chiapas, Mexico. *Arizona Geol. Soc. Dig.* XI 155–168.
- de Ignacio, C., Castañeiras, P., Márquez, A., Oyarzún, R., Lillo, J., López, I., 2003. El Chichón Volcano (Chiapas Volcanic Belt, Mexico) Transitional Calc-Alkaline to Adakitic-like Magmatism: Petrologic and Tectonic Implications. *Int. Geol. Rev.* 45, 1020–1028. <https://doi.org/10.2747/0020-6814.45.11.1020>.
- DeMets, C., Gordon, R.G., Argus, D.F., 2010. Geologically current plate motions. *Geophys. J. Int.* 181, 1–80. <https://doi.org/10.1111/j.1365-246X.2009.04491.x>.
- Dougherty, S.L., Clayton, R.W., 2014. Seismicity and structure in Central Mexico: evidence for a possible slab tear in the South Cocos plate. *J. Geophys. Res. Solid Earth* 119, 3424–3447. <https://doi.org/10.1002/2013JB010883>.
- Faccenda, M., Capitanio, F.A., 2012. Development of mantle seismic anisotropy during subduction-induced 3-D flow. *Geophys. Res. Lett.* 39, 1–5. <https://doi.org/10.1029/2012GL051988>.
- Faccenda, M., Burlini, L., Gerya, T., Mainprice, D., 2008. Fault-induced seismic anisotropy by hydration in subducting oceanic plates. *Nature* 455, 1097–1101.
- Fasola, S., Brudzinski, M.R., Ghose, N., Solada, K., Sit, S., Cabral-Cano, E., Arciniega-Ceballos, A., Kelly, N., Jensen, K., 2016. New perspective on the transition from flat to steeper subduction in Oaxaca, Mexico, based on seismicity, nonvolcanic tremor, and slow slip. *J. Geophys. Res. Solid Earth* 121, 1835–1848. <https://doi.org/10.1002/2015JB012709>.
- Ferrari, L., Orozco-Esquivel, T., Manea, V.C., Manea, M., 2012. The dynamic history of the Trans-Mexican Volcanic Belt and the Mexico subduction zone. *Tectonophysics* 522–523, 122–149. <https://doi.org/10.1016/j.tecto.2011.09.018>.
- Frederiksen, A.W., Bostock, M.G., 2000. Modelling teleseismic waves in dipping anisotropic structures. *Geophys. J. Int.* 141, 401–412. <https://doi.org/10.1046/j.1365-246X.2000.00090.x>.
- Gill, J.B., 1981. *Orogenic Andesites and Plate Tectonics, Minerals and Rocks*, vol. 16. Springer-Verlag, Berlin, Germany.
- Gripp, A.E., Gordon, R.G., 2002. Young tracks of hotspots and current plate velocities. *Geophys. J. Int.* 150, 321–361. <https://doi.org/10.1046/j.1365-246X.2002.01627.x>.
- Hayes, G.P., Moore, G.L., Portner, D.E., Hearne, M., Flamme, H., Furtney, M., Smoczyk, G.M., 2018. Slab2, a comprehensive subduction zone geometry model. *Science* 362, 58–61. <https://doi.org/10.1126/science.aat4723>.
- Husker, A., Davis, P.M., 2009. Tomography and thermal state of the Cocos plate subduction beneath Mexico City. *J. Geophys. Res. Solid Earth* 114, 1–15. <https://doi.org/10.1029/2008JB006039>.
- Hyndman, R.D., Peacock, S.M., 2003. Serpentinitization of the Forearc Mantle, 212, pp. 417–432. [https://doi.org/10.1016/S0012-821X\(03\)00263-2](https://doi.org/10.1016/S0012-821X(03)00263-2).
- Jung, H., 2011. Seismic anisotropy produced by serpentine in mantle wedge. *Earth Planet. Sci. Lett.* 307, 535–543. <https://doi.org/10.1016/j.epsl.2011.05.041>.
- Jung, H., Karato, S.I., 2001. Water-induced fabric transitions in olivine. *Science* 293, 1460–1463. <https://doi.org/10.1126/science.1062235>.
- Jung, H., Katayama, I., Jiang, Z., Hiraga, T., Karato, S., 2006. Effect of water and stress on the lattice-preferred orientation of olivine. *Tectonophysics* 421, 1–22. <https://doi.org/10.1016/j.tecto.2006.02.011>.
- Kaneshima, S., 1990. Origin of crustal anisotropy: Shear wave splitting studies in Japan. *J. Geophys. Res.* 95, 11121–11133.
- Kanjorski, M.N., 2003. Cocos plate structure along the Middle America subduction zone off Oaxaca and Guerrero, Mexico: Influence of subducting plate morphology on tectonics and seismicity. Ph. D. Dissertation. University of California, San Diego, p. 202.
- Karato, S.-I., Jung, H., Katayama, I., Skemer, P., 2008. Geodynamic significance of seismic anisotropy of the upper mantle: new insights from laboratory studies. *Annu. Rev. Earth Planet. Sci.* 36, 59–95. <https://doi.org/10.1146/annurev.earth.36.031207.124120>.
- Katayama, I., Hirauchi, K., Michibayashi, K., Ando, J., 2009. Trench-parallel anisotropy produced by serpentine deformation in the hydrated mantle wedge. *Nature* 461, 1114–1118. <https://doi.org/10.1038/nature08513>.
- Kim, Y., Clayton, R.W., Jackson, J.M., 2010. Geometry and Seismic Properties of the Subducting Cocos Plate in Central Mexico, 115, pp. 1–22. <https://doi.org/10.1029/2009JB006942>.
- Kim, Y., Clayton, R.W., Keppie, F., 2011. Evidence of a collision between the Yucatán Block and Mexico in the Miocene. *Geophys. J. Int.* 187, 989–1000. <https://doi.org/10.1111/j.1365-246X.2011.05191.x>.
- Kincaid, C., Griffiths, R.W., 2004. Variability in flow and temperatures within mantle subduction zones. *Geochemistry, Geophys. Geosystems* 5. <https://doi.org/10.1029/2003GC000666>.
- Klitgord, K.D., Mammerickx, J., 1982. Northern East Pacific rise: magnetic anomaly and bathymetric framework. *J. Geophys. Res.* 87, 6725–6750.
- Kneller, E.A., van Keken, P.E., Karato, S.I., Park, J., 2005. B-type olivine fabric in the mantle wedge: Insights from high-resolution non-Newtonian subduction zone models. *Earth Planet. Sci. Lett.* 237, 781–797. <https://doi.org/10.1016/j.epsl.2005.06.049>.
- León Soto, G., Valenzuela, R.W., Arceo, R., Huesca-Pérez, E., Rosas, R.V., 2021. Teleseismic measurements of upper mantle shear wave anisotropy in the Isthmus of Tehuantepec, Mexico. *Geophys. J. Int.* 227, 1784–1794. <https://doi.org/10.1093/gji/gjab301>.
- Long, M.D., 2013. Constraints on subduction geodynamics from seismic anisotropy. *Rev. Geophys.* 51, 76–112. <https://doi.org/10.1002/rog.20008>.
- Long, M.D., Silver, P.G., 2008. The subduction zone flow field from seismic anisotropy: a global view. *Science* 319, 315–318. <https://doi.org/10.1126/science.1150809>.
- Long, M.D., Silver, P.G., 2009. Mantle flow in subduction systems: the subslab flow field and implications for mantle dynamics. *J. Geophys. Res.* 114, B10312 <https://doi.org/10.1029/2008JB006200>.
- Long, M.D., Wirth, E.A., 2013. Mantle flow in subduction systems: the mantle wedge flow field and implications for wedge processes. *J. Geophys. Res. Solid Earth* 118, 583–606. <https://doi.org/10.1002/jgrb.50063>.
- Lynner, C., Long, M.D., 2013. Sub-slab seismic anisotropy and mantle flow beneath the Caribbean and Scotia subduction zones: Effects of slab morphology and kinematics. *Earth Planet. Sci. Lett.* 361, 367–378. <https://doi.org/10.1016/j.epsl.2012.11.007>.
- Manea, V.C., Manea, M., 2006. Origin of the modern Chiapanecan Volcanic arc in southern México inferred from thermal models. *Spec. Pap. Geol. Soc.* 412, 27–38. [https://doi.org/10.1130/2006.2412\(02\).](https://doi.org/10.1130/2006.2412(02).)
- Manea, M., Manea, V.C., 2008. On the origin of El Chichón volcano and subduction of Tehuantepec Ridge: a geodynamical perspective. *J. Volcanol. Geotherm. Res.* 175, 459–471. <https://doi.org/10.1016/j.jvolgeores.2008.02.028>.
- Manea, M., Manea, V.C., Ferrari, L., Kostoglodov, V., Bandy, W.L., 2005a. Tectonic evolution of the Tehuantepec Ridge. *Earth Planet. Sci. Lett.* 238, 64–77. <https://doi.org/10.1016/j.epsl.2005.06.060>.
- Manea, M., Manea, V.C., Kostoglodov, V., Guzmán-Speziale, M., 2005b. Elastic thickness of the oceanic lithosphere beneath Tehuantepec ridge. *Geofis. Int.* 44, 157–168.
- Manea, M., Manea, V.C., Ferrari, L., Orozco-Esquivel, T., 2019. Delamination of subcrustal lithosphere beneath the Isthmus of Tehuantepec, Mexico: Insights from numeric modelling. *J. Geodyn.* 129, 262–274. <https://doi.org/10.1016/j.jog.2018.09.002>.

- Melgar, D., Pérez-Campos, X., 2011. Imaging the moho and subducted oceanic crust at the isthmus of Tehuantepec, Mexico, from receiver functions. *Pure Appl. Geophys.* 168, 1449–1460. <https://doi.org/10.1007/s00024-010-0199-5>.
- Mookherjee, M., Capitani, G.C., 2011. Trench parallel anisotropy and large delay times: Elasticity and anisotropy of antigorite at high pressures. *Geophys. Res. Lett.* 38, <https://doi.org/10.1029/2011GL047160>.
- Nava Lara, S.V., Manea, V.C., 2022. Numerical models for slab tearing beneath southern Mexico and northern Central America. *J. South Am. Earth Sci.* 115, 103771. <https://doi.org/10.1016/j.jsames.2022.103771>.
- Nelson, S., Gonzalez-Caver, E., Kyser, T., 1995. Constraints on the origin of alkaline and calc-alkaline magmas from the Tuxtla Volcanic Field, Veracruz, Mexico. *Contrib. Miner. Pet.* 122, 191–211. <https://doi.org/10.1007/s004100050121>.
- Pardo, M., Suarez, G., 1995. Shape of the subducted Rivera and Cocos plates in southern Mexico: seismic and tectonic implications. *J. Geophys. Res.* 100 <https://doi.org/10.1029/95jb00919>.
- Pérez-Campos, X., Kim, Y.H., Husker, A., Davis, P.M., Clayton, R.W., Iglesias, A., Pacheco, J.F., Singh, S.K., Manea, V.C., Gurnis, M., 2008. Horizontal subduction and truncation of the Cocos Plate beneath Central Mexico. *Geophys. Res. Lett.* 35, 1–6. <https://doi.org/10.1029/2008GL035127>.
- Pérez-Campos, X., Espíndola, V.H., Pérez, J., Estrada, J.A., Monroy, C.C., Bello, D., González-López, A., Avila, D.G., Esparza, M.G.C.R., Maldonado, R., Tan, Y., Rasilla, I.R., Rosas, M.Á.V., Cruz, J.L., Cárdenas, A., Estrada, F.N., Hurtado, A., De Jesús Mendoza Carvajal, A., Montoya-Quintanar, E., Pérez-Velázquez, M.A., 2018. The Mexican National seismological service: an overview. *Seismol. Res. Lett.* 89, 318–323. <https://doi.org/10.1785/0220170186>.
- Rebollar, C.J., Espíndola, V.H., Uribe, A., Mendoza, A., Pérez-Vertti, A., 1999. Distributions of stresses and geometry of the Wadati-Benioff zone under Chiapas, Mexico. *Geofis. Int.* 38, 95–106.
- Rodríguez-Domínguez, M., Pérez-Campos, X., Montecalegre-Cázares, C., Clayton, R.W., Cabral-Cano, E., 2019. Crustal structure variations in south-Central Mexico from receiver functions. *Geophys. J. Int.* 219, 2174–2186. <https://doi.org/10.1093/gji/ggz434>.
- Rodríguez-Pérez, Q., 2007. Estructura tridimensional de velocidades para el sureste de México, mediante el análisis de trazado de rayos sísmicos de sismos regionales. M. Sc. thesis. Instituto de Geofísica, Universidad Nacional Autónoma de México, Mexico City, Mexico, p. 88.
- Rümpker, G., Silver, P.G., 1998. Apparent shear-wave splitting parameters in the presence of vertically varying anisotropy. *Geophys. J. Int.* 135, 790–800. <https://doi.org/10.1046/j.1365-246X.1998.00660.x>.
- Savage, M.K., 1999. Seismic anisotropy and mantle deformation. *Rev. Geophys.* 37, 65–106. <https://doi.org/10.1029/98RG02075>.
- Silver, P.G., 1996. Seismic anisotropy beneath the continents: probing the depths of Geology. *Annu. Rev. Earth Planet. Sci.* 24, 385–432. <https://doi.org/10.1146/annurev.earth.24.1.385>.
- Silver, P.G., Chan, W.W., 1991. Shear Wave Splitting and Subcontinental Mantle Deformation. *J. Geophys. Res.* 96, 16429–16454.
- Silver, P.G., Savage, M.K., 1994. The interpretation of shear-wave splitting parameters in the presence of two anisotropic layers. *Geophys. J. Int.* 119, 949–963.
- Song, T.A., Kawakatsu, H., 2012. Subduction of oceanic asthenosphere: evidence from sub-slab seismic anisotropy. *Geophys. Res. Lett.* 39, 1–6. <https://doi.org/10.1029/2012GL052639>.
- SSN, 2021a. Servicio Sismológico Nacional, Instituto de Geofísica, Universidad Nacional Autónoma de México, Mexico City, Mexico. Revised Earthquake Catalog. <https://doi.org/10.21766/SSNMX/EC/MX>. Available on. <http://www2.ssn.unam.mx:8080/catalogo/>.
- SSN, 2021b. Servicio Sismológico Nacional, Instituto de Geofísica, Universidad Nacional Autónoma de México, Mexico City, Mexico. <https://doi.org/10.21766/SSNMX/SN/MX>.
- Suarez, G., Singh, S.K., 1986. Tectonic interpretation of the Trans-Mexican Volcanic Belt - Discussion. *Tectonophysics* 127, 155–158.
- Teanby, N.A., Kendall, J., Van Der Baan, M., 2004. Automation of shear-wave splitting measurements using cluster analysis. *Bull. Seism. Soc. Am.* 94, 453–463.
- Valenzuela, R.W., León Soto, G., 2017. Shear wave splitting and mantle flow in Mexico: What have we learned? *Geofis. Int.* 56, 187–217. <https://doi.org/10.19155/geofint.2017.056.2.1765>.
- van Benthem, S.A.C., Valenzuela, R.W., Ponce, G.J., 2013. Measurements of upper mantle shear wave anisotropy from a permanent network in southern Mexico. *Geofis. Int.* 52, 385–402. [https://doi.org/10.1016/S0016-7169\(13\)71485-5](https://doi.org/10.1016/S0016-7169(13)71485-5).
- Velasco, A., Karplus, M., 2017. Rapid aftershock deployment for the September 2017 M=8.1 and M=7.1 earthquakes in Mexico (RADSEM). Int. Fed. Digit. Seismogr. Networks. https://doi.org/10.7914/SN/ZB_2017.
- Wessel, P., Smith, W.H.F., 1998. New, improved version of Generic Mapping Tools released. *EOS Trans. AGU* 79, 579.
- Wilson, D.S., 1996. Fastest known spreading on the Miocene Cocos-Pacific plate boundary. *Geophys. Res. Lett.* 23, 3003–3006. <https://doi.org/10.1029/96GL02893>.
- Wolfe, C.J., Silver, P.G., 1998. Seismic anisotropy of oceanic upper mantle: Shear wave splitting methodologies and observations. *J. Geophys. Res. Solid Earth* 103, 749–771. <https://doi.org/10.1029/97jb02023>.
- Wüstefeld, A., Bokelmann, G., Zaroli, C., Barruol, G., 2008. SplitLab: a shear-wave splitting environment in Matlab. *Comput. Geosci.* 34, 515–528. <https://doi.org/10.1016/j.cageo.2007.08.002>.
- Zhang, S., Karato, S., 1995. Lattice preferred orientation of olivine aggregates in simple shear. *Nature* 375, 774–777.